



Neutral-charged-particle Collisions as the Mechanism for Accretion Disk Angular Momentum Transport

Yang Zhang and Paul M. Bellan

California Institute of Technology, Pasadena, CA 91125, USA; yangzhan@caltech.edu

Received 2021 November 24; revised 2022 March 3; accepted 2022 March 21; published 2022 May 17

Abstract

The matter in an accretion disk must lose angular momentum when moving radially inwards but how this works has long been a mystery. By calculating the trajectories of individual colliding neutrals, ions, and electrons in a weakly ionized 2D plasma containing gravitational and magnetic fields, we numerically simulate accretion disk dynamics at the particle level. As predicted by Lagrangian mechanics, the fundamental conserved global quantity is the total canonical angular momentum, not the ordinary angular momentum. When the Kepler angular velocity and the magnetic field have opposite polarity, collisions between neutrals and charged particles cause: (i) ions to move radially inwards, (ii) electrons to move radially outwards, (iii) neutrals to lose ordinary angular momentum, and (iv) charged particles to gain canonical angular momentum. Neutrals thus spiral inward due to their decrease of ordinary angular momentum while the accumulation of ions at small radius and accumulation of electrons at large radius produces a radially outward electric field. In 3D, this radial electric field would drive an out-of-plane poloidal current that produces the magnetic forces that drive bidirectional astrophysical jets. Because this neutral angular momentum loss depends only on neutrals colliding with charged particles, it should be ubiquitous. Quantitative scaling of the model using plausible disk density, temperature, and magnetic field strength gives an accretion rate of 3×10^{-8} solar mass per year, which is in good agreement with observed accretion rates.

Unified Astronomy Thesaurus concepts: [Accretion \(14\)](#); [Stellar accretion \(1578\)](#); [Jets \(870\)](#); [Plasma jets \(1263\)](#); [Protoplanetary disks \(1300\)](#); [Circumstellar disks \(235\)](#); [Plasma astrophysics \(1261\)](#)

Supporting material: animations

1. Introduction

Protoplanetary disks (PPDs) are thin, weakly ionized, cold accretion disks existing during the early life of a star and typically have associated poloidal magnetic fields and bidirectional astrophysical jets. PPDs have inner radii of a few astronomical units, outer radii of 10–100 au, accretion rates of 10^{-9} to $10^{-7} M_{\odot} \text{ yr}^{-1}$ (Gullbring et al. 1998), and poloidal magnetic fields >1 mG (Harrison et al. 2021). Because accreting particles must shed angular momentum to satisfy energy constraints, accretion must involve outward transport of angular momentum (Balbus 2003), but how this works has been a long-standing mystery. Classical viscosity is insufficient to provide the required angular momentum transport, so efforts have been directed toward finding stronger transport mechanisms. Shakura & Sunyaev (1973) proposed turbulence but did not suggest a source for the postulated turbulence. Balbus & Hawley (1991) derived the magnetorotational instability (MRI) and proposed the MRI as the source of turbulence enhancing angular momentum transport. However, Flaherty et al. (2017) measured actual turbulent levels in a PPD, and found “there is little turbulence throughout the vertical extent of the disk, contrary to theoretical predictions based on the magnetorotational instability.” Ji et al. (2006) constructed a laboratory device designed to demonstrate the MRI, but MRI has not been detected so far; Ji & Balbus (2013) stated, “To date, however,

the MRI has been difficult to identify unambiguously, even though the required threshold conditions have been exceeded.”

As an alternate to turbulence and MRI, Bellan (2016) argued that because the accretion disk is an axisymmetric electromagnetic-gravitational system, the fundamental conserved quantity is not the *ordinary* angular momentum (OAM) $mr v_{\theta}$ but rather the *canonical* angular momentum (CAM) $mr v_{\theta} + q\psi/2\pi$ where q is the charge, and ψ is the poloidal magnetic flux.

We report here particle simulations of a weakly ionized, collisional accretion disk. The simulated accretion disk is composed of “hard-disk” neutrals, ions, and electrons (because the simulation is in 2D, the particles are “hard disks” rather than “hard spheres”; note that the word “disk” is being used in two different contexts—accretion disk and particle disk—which should not be confused). It is found that in the presence of collisions, the total accretion disk CAM is conserved but the total OAM is not. The numerical simulation shows that collisions cause the charged particle CAM to increase with a corresponding reduction of the neutral OAM so that total CAM is conserved. In accordance with their decreased OAM, neutrals spiral inwards, i.e., accrete. The microscopic details of the OAM and CAM transfer are explained by direct calculation of the average radial velocity of a charged particle as a result of collisions with Kepler-orbiting neutrals. A radially outward electric field develops as a result of the radial inward/outward motion of the ions/electrons, and this electric field is just what is required to drive the bidirectional out-of-plane electric currents flowing along bidirectional astrophysical jets. The simulations and their interpretation provide a ubiquitous, straightforward model of angular momentum shedding and jet drive mechanism (Bellan 2016).



Original content from this work may be used under the terms of the [Creative Commons Attribution 4.0 licence](#). Any further distribution of this work must maintain attribution to the author(s) and the title of the work, journal citation and DOI.

2. Simulation Method

The simulation has a central body with mass M_* at the origin of a cylindrical coordinate system $\{r, \theta, z\}$ and a uniform magnetic field $\mathbf{B} = B\hat{z}$ so the poloidal flux is $\psi = B\pi r^2$. Surrounding the central body are a large number of particles represented by hard disks restricted to the $z = 0$ plane. When not colliding, the equation of motion for a particle with mass m and charge q is

$$m \frac{d\mathbf{v}}{dt} = q\mathbf{v} \times \mathbf{B} - \frac{GM_*m}{r^2} \hat{r}. \quad (1)$$

Using reference parameters $r_0 = 1$ au, $v_{K0} = \sqrt{GM_*/r_0}$, $\omega_{K0} = \sqrt{GM_*/r_0^3}$, normalized quantities $\bar{r} = r/r_0$, $\bar{\mathbf{v}} = \mathbf{v}/v_{K0}$, $\bar{t} = \omega_{K0}t$, $\bar{\omega}_c = q\mathbf{B}/m$, and $\bar{\omega}_c = \omega_c/\omega_{K0}$ are defined so that Equation (1) becomes

$$\frac{d\bar{\mathbf{v}}}{d\bar{t}} = \bar{\omega}_c \bar{\mathbf{v}} \times \hat{z} - \frac{1}{\bar{r}^2} \hat{r}. \quad (2)$$

The hard-disk particle model means that particles do not interact except when colliding. Particles are assumed to be disks having radius a and center at \mathbf{r}_i where $i = 1$ to N and N is the number of particles. A collision occurs between particle i and particle j when $|\mathbf{r}_i - \mathbf{r}_j| < 2a$. The velocity change of particle i after a collision is

$$\delta \mathbf{v}_i = -\frac{2m_j}{m_i + m_j} (\mathbf{v}_{ij} \cdot \hat{\mathbf{n}}_{ij}) \hat{\mathbf{n}}_{ij}, \quad (3)$$

where $\mathbf{v}_{ij} = \mathbf{v}_i - \mathbf{v}_j$ and $\hat{\mathbf{n}}_{ij} = \frac{\mathbf{r}_i - \mathbf{r}_j}{|\mathbf{r}_i - \mathbf{r}_j|}$.

On defining \mathbf{u}_i as the mean velocity of species i , the frictional drag frequency ν_{ij} of species j on species i is defined by $d\mathbf{u}_i/dt = -\nu_{ij}(\mathbf{u}_i - \mathbf{u}_j)$; integrating this over a short time T gives

$$\Delta \mathbf{u}_i = -\nu_{ij} T (\mathbf{u}_i - \mathbf{u}_j). \quad (4)$$

If a particle makes S collisions in a time T then, its change in velocity will be $\Delta \mathbf{v}_i = \sum_{k=1}^S \delta \mathbf{v}_i(k)$. The change of the species mean velocity will be

$$\Delta \mathbf{u}_i = \left\langle \sum_{k=1}^S \delta \mathbf{v}_i(k) \right\rangle = -\sum_{k=1}^S \frac{2m_j}{m_i + m_j} \langle (\mathbf{v}_{ij} \cdot \hat{\mathbf{n}}_{ij}) \hat{\mathbf{n}}_{ij} \rangle \quad (5)$$

where the angle brackets denote averaging over particles and over directions $\hat{\mathbf{n}}_{ij}$. By defining $\hat{\mathbf{p}} = \hat{z} \times \hat{\mathbf{v}}_{ij}$ where \hat{z} is out of plane, then $\hat{\mathbf{n}}_{ij} = \hat{\mathbf{v}}_{ij} \cos \phi + \hat{\mathbf{p}} \sin \phi$ where ϕ is a random angle that differs for each of the S collisions. Since $(\mathbf{v}_i - \mathbf{v}_j) \cdot \hat{\mathbf{n}}_{ij} = |\mathbf{v}_i - \mathbf{v}_j| \cos \phi$, then ϕ averaging of $(\mathbf{v}_i - \mathbf{v}_j) \cdot \hat{\mathbf{n}}_{ij} \hat{\mathbf{n}}_{ij}$ gives $(\mathbf{v}_i - \mathbf{v}_j) \cdot \hat{\mathbf{n}}_{ij} \hat{\mathbf{n}}_{ij} = (\mathbf{v}_i - \mathbf{v}_j) \cos^2 \phi$. Averaging over many particles gives $\langle (\mathbf{v}_i - \mathbf{v}_j) \cdot \hat{\mathbf{n}}_{ij} \hat{\mathbf{n}}_{ij} \rangle = (\mathbf{u}_i - \mathbf{u}_j)/2$ so combining Equations (4) and (5) gives

$$\nu_{ij} = \frac{S}{T} \frac{m_j}{m_i + m_j}. \quad (6)$$

The collisional drag frequency ν_{ij} is thus determined from the numerical simulation by counting how many collisions S are experienced by a particle in a time T and then using Equation (6). The ergodic assumption that the friction of a single particle over many collisions is the same as the average instantaneous friction experienced by many particles allows this determination to be made by following a single numerical particle.

A reflective boundary at an inner radius $\bar{r} = 0.1 - \bar{a}$ is used to avoid the infinite gravitational force when particles move close to the origin. This reflective boundary means that a particle is reflected back with an opposite radial velocity when it tries to penetrate inside a circle having radius $\bar{r} = 0.1$. Because this reflection is radial, it conserves both canonical and ordinary angular momentum. There is no boundary at large radius. Unless specified otherwise, $\bar{a} = 0.01$, and the number of particles is $N = 16,128$. The ion mass is set to $\bar{m}_i = m_i/m_n = 1$, and the electron mass is set to $\bar{m}_e = m_e/m_n = 0.1$. The simulation starts at $\bar{t} = 0$ with particles located in concentric circles ranging from $\bar{r} = 0.3$ to $\bar{r} = 1.9$, with a spacing $\bar{d} = 2.5\bar{a}$ between adjacent concentric circles. The particles are arranged at $\bar{t} = 0$ with uniform azimuthal spacing on each circle with interparticle angular separation $\Delta\theta = 2\pi/[2\pi\bar{r}/\bar{d}]$ where $[2\pi\bar{r}/\bar{d}]$ means the nearest integer greater than or equal to $2\pi\bar{r}/\bar{d}$. Particles are assigned an initial Kepler velocity with $\bar{\mathbf{v}} = \sqrt{1/\bar{r}}\hat{\theta}$. The magnetic field direction is opposite to the Kepler rotation sense, i.e., $B < 0$. A Boris method (Boris 1970) is used for pushing the particles, and the time step is $\Delta\bar{t} = 10^{-4}$. The total system dimensionless CAM (Bellan 2016) is

$$\begin{aligned} \bar{P}_\theta &= \frac{P_\theta}{m_n r_0^2 \omega_{K0}} = \frac{\sum_{j=1}^N (m_j r_j^2 \dot{\theta}_j + \frac{1}{2} q_j B r_j^2)}{m_n r_0^2 \omega_{K0}} \\ &= \sum_{j=1}^N \left(\bar{m}_j \bar{r}_j^2 \bar{\theta}_j + \frac{1}{2} \bar{m}_j \bar{\omega}_{cj} \bar{r}_j^2 \right), \end{aligned} \quad (7)$$

and the total system dimensionless OAM is

$$\bar{L}_\theta = \frac{L_\theta}{m_n r_0^2 \omega_{K0}} = \frac{\sum_{j=1}^N m_j r_j^2 \dot{\theta}_j}{m_n r_0^2 \omega_{K0}} = \sum_{j=1}^N \bar{m}_j \bar{r}_j^2 \bar{\theta}_j. \quad (8)$$

3. Main Results

Figure 1 displays simulation results when there is an ion (red dot) and an electron (black dot) and a large number of neutrals (blue and gray dots). The neutrals neighboring the ion–electron pair at $\bar{t} = 0$ are shown as dark blue dots. The ion is at initial position $(\bar{r}, \theta) = (1, 0)$ with $\bar{\omega}_{ci} = -50$. The electron is at initial position $(\bar{r}, \theta) = (1.025, 0)$ with $\bar{\omega}_{ce} = +500$. By counting the number of collisions made by the electrons and ions in one Kepler period, it is found that $\bar{\nu}_{in} = 56.6$ and $\bar{\nu}_{en} = 253.1$. Figures 1(a)–(d) show the system state at $\bar{t} = 0, 0.34, 0.68$ and 1. Figure 1(e) displays the time dependence of the total system CAM \bar{P}_θ as defined by Equation (7) and the total system OAM \bar{L}_θ as defined by Equation (8). Figure 1(e) thus verifies that the basic conserved quantity is not the system OAM but rather the system CAM. Figure 1(f) plots the ion and electron radial positions and shows that the ion moves radially inwards while the electron moves radially outwards. Figure 1(g) plots the time dependence of the CAM of the ion and of the electron and shows that the ion and electron CAM are both increasing. Because total system CAM \bar{P}_θ is conserved and the ion and electron CAM are increasing, the OAM of the neutrals decreases as shown in Figure 1(h). Effectively, the neutral OAM is transferred to the ion and electron CAM as the system evolves. Since OAM scales as $r^{1/2}$, removing OAM from neutrals corresponds to the neutrals accreting toward the star. Neutral–neutral collisions will conserve neutral OAM, so it is possible for some neutrals to move inwards while others move outwards in a way that conserves OAM; unlike collisions

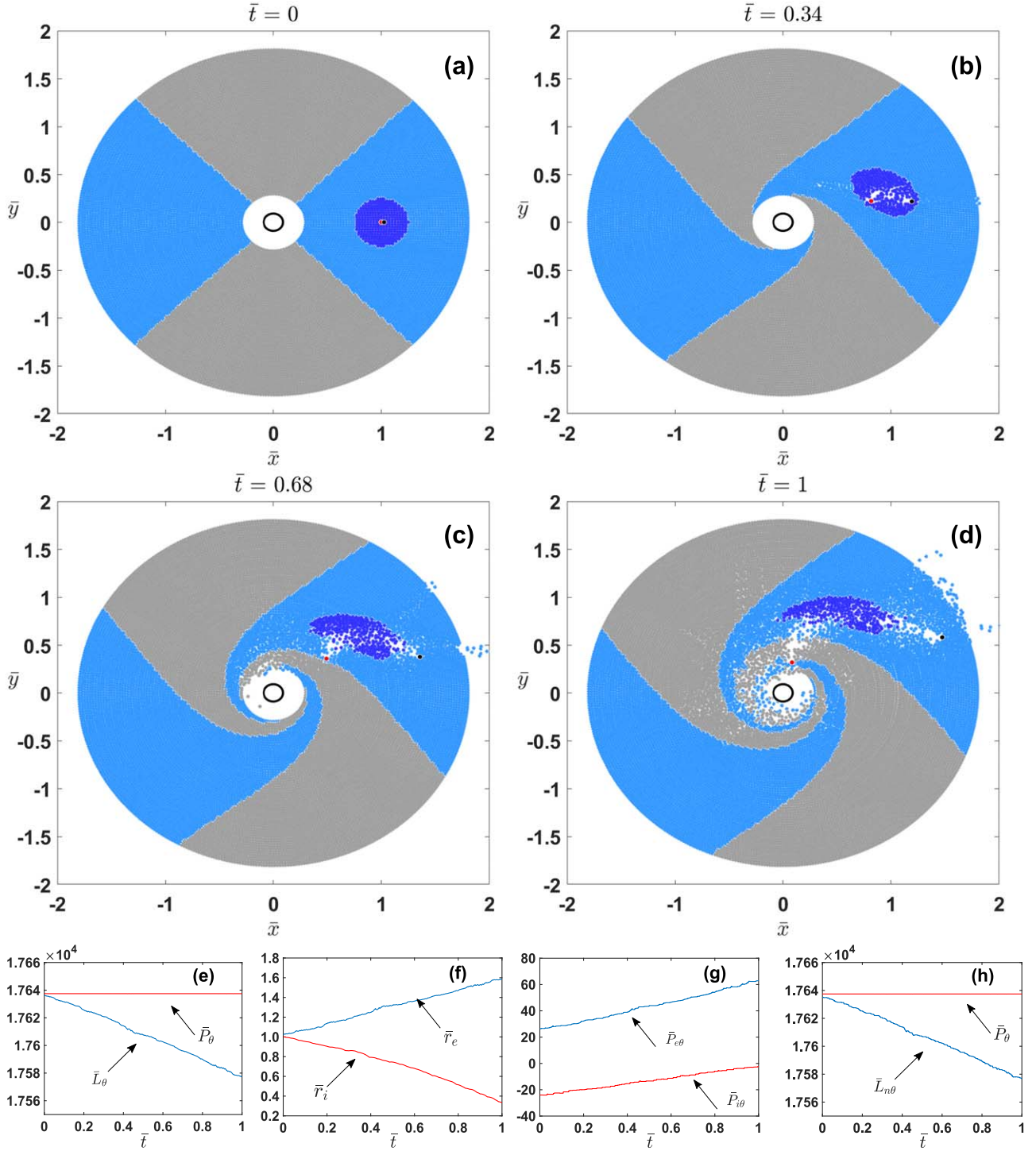


Figure 1. Simulation results when there is an electron–ion pair in the system. The ion is at initial position $(\bar{r}, \theta) = (1, 0)$ with $\bar{\omega}_{ci} = -50$ and $\bar{v}_{in} = 56.6$. The electron is at initial position $(\bar{r}, \theta) = (1.025, 0)$ with $\bar{\omega}_{ce} = +500$ and $\bar{v}_{en} = 253.1$. (a)–(d) The particle trajectories of the whole system at time $\bar{t} = 0, 0.34, 0.68$ and 1. Neutral particles are blue and gray. The ion is red, and the electron is black. The neutrals surrounding the electron–ion pair at $\bar{t} = 0$ are dark blue. The full trajectories video ($\bar{t} = 0$ to 1) is shown as an animation. (e) The total canonical angular momentum of the system and the total ordinary angular momentum of the system. (f) The radial positions of the ion and electron. (g) The canonical angular momentum of the ion and electron. (h) The ordinary angular momentum of the neutrals and the total canonical angular momentum of the system.

(An animation of this figure is available.)

with charged particles, this process will not cause global loss of neutral OAM.

We now explain why an ion and an electron have opposite average radial displacement as a result of collisions with neutrals and then relate this to angular momentum transport.

The equation of motion for charged particles σ moving in a sea of neutral particles is

$$\frac{d\mathbf{u}_\sigma}{dt} \approx \omega_{c\sigma} \mathbf{u}_\sigma \times \hat{\mathbf{z}} - \nu_{\sigma n} (\mathbf{u}_\sigma - \mathbf{u}_n) \quad (9)$$

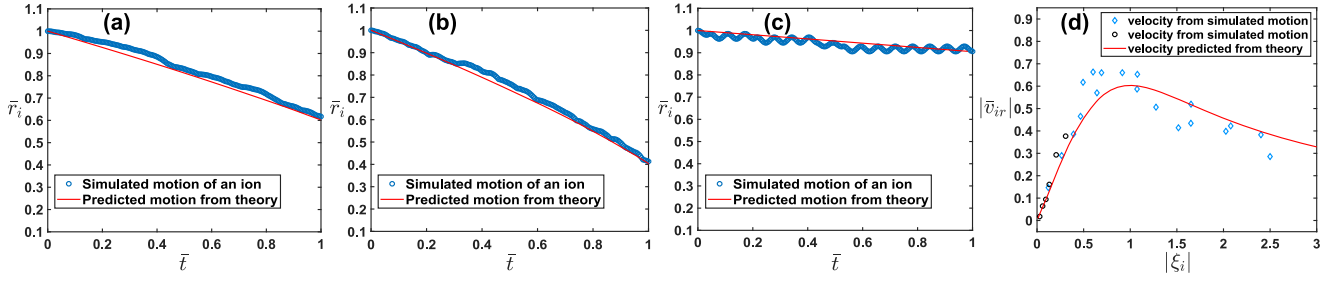


Figure 2. (a)–(c) Comparison between the simulated motion of one ion in the system (blue circles) and the predicted motion from Equation (13) (red lines). In (a) to (c) respectively, $\bar{\omega}_{ci} = -12, -50, -100$, $\bar{v}_{in} = 28.8, 53.6, 9.4$, which give $\xi = -2.40, -1.07, -0.09$. (d) Comparison between the simulated velocity of one ion in the system (blue diamonds and black circles) and the predicted velocity from Equation (12) (red lines) with $|\bar{v}_{ir}| = |\bar{r}_i(\bar{t} = 1) - \bar{r}_i(\bar{t} = 0)|$. For (c) and the black circles in (d), the simulation has $\bar{a} = 0.025$ and $\bar{d} = 4\bar{a}$ with $N = 1183$ particles arranged on concentric circles from $\bar{r} = 0.3$ to $\bar{r} = 1.9$. The two-dimensional particle trajectories in (c) are available as an animation. The animation runs from $\bar{t} = 0$ to 2.

(An animation of this figure is available.)

where $\nu_{\sigma n}$ is given by Equation (6). The gravitational force on the charged particles is ignored because $|\bar{\omega}_{c\sigma}| \gg 1$. The exact solution for Equation (9) is

$$\mathbf{u}_\sigma = (\mathbf{u}_L \cos(\omega_{c\sigma} t) + \mathbf{u}_L \times \hat{z} \sin(\omega_{c\sigma} t)) e^{-\nu_{\sigma n} t} + \frac{1}{1 + \frac{\nu_{\sigma n}^2}{\omega_{c\sigma}^2}} \left(\frac{\nu_{\sigma n}}{\omega_{c\sigma}} \mathbf{u}_n \times \hat{z} + \frac{\nu_{\sigma n}^2}{\omega_{c\sigma}^2} \mathbf{u}_n \right). \quad (10)$$

On time-averaging over a cyclotron period, the terms containing $\cos(\omega_{c\sigma} t)$ and $\sin(\omega_{c\sigma} t)$ vanish. On defining $\xi_\sigma = \frac{\nu_{\sigma n}}{\omega_{c\sigma}}$, the time-averaged charged particle velocity is

$$\mathbf{u}_\sigma = \frac{\xi_\sigma \mathbf{u}_n \times \hat{z} + \xi_\sigma^2 \mathbf{u}_n}{1 + \xi_\sigma^2}. \quad (11)$$

We presume that the neutrals are in Keplerian motion, so \mathbf{u}_n is in the θ direction. The radial component of the time-averaged charged particle velocity is thus

$$u_{\sigma r} = \frac{\xi_\sigma}{1 + \xi_\sigma^2} u_{n\theta}. \quad (12)$$

Because ions and electrons have opposite polarity, their $\omega_{c\sigma}$ and hence their ξ_σ have opposite signs, so u_{ir} and u_{er} have opposite signs. The simulation has $B < 0$ and Kepler rotation with $u_{n\theta} > 0$. Equation (12) gives negative radial velocity for ions and positive for electrons, so ions move radially inwards and electrons move radially outwards as seen in the simulations. Because $B < 0$, the CAM magnetic component $qBr^2/2$ thus increases for both electrons and ions. Furthermore, it is seen that the radial velocity of charged particles of type σ has a maximum of $1/2$ which occurs when $|\xi_\sigma| = 1$. Because the total CAM of the two particles involved in each collision is conserved, the system total CAM is conserved. The OAM of the neutrals must decrease as a result of collisions with both electrons and ions because, on average, collisions cause an increase in the CAM of both electrons and ions. The mechanism is insensitive to the polarity of the magnetic field, because if $B > 0$, Equation (12) shows ions move radially outwards and electrons move radially inwards, so the CAM of the charged particles increases, in which case the neutral OAM will again decrease.

Assuming a constant collision frequency and using $\bar{u}_{n\theta} = 1/\bar{r}^{1/2}$, Equation (12) can be integrated to give

$$\bar{r}_\sigma(\bar{t}) = \left(\frac{3}{2} \frac{\xi_\sigma}{1 + \xi_\sigma^2} \bar{t} + \bar{r}_\sigma^3(\bar{t} = 0) \right)^{2/3}. \quad (13)$$

Figures 2(a)–(c) compare the time dependence of the radial position of an ion from a simulation with the dependence predicted by Equation (13); the ion initial position is $(\bar{r}, \theta) = (1, 0)$. Figure 2(d) presents the ξ_i dependence of the average radial velocity $|\bar{v}_{ir}| = |\bar{r}_i(\bar{t} = 1) - \bar{r}_i(\bar{t} = 0)|$. The simulation motion and radial velocity agree well with Equation (13) and also confirm that the ion radial velocity has maximum value when $|\xi| = 1$. The discrepancy of some simulated points in Figure 2(d) is presumed to be from the friction collision force approximation and radial velocity of colliding neutrals. The friction collision force is derived from averaging over the finite number of collisions, so if the number of collisions is not large, there will be significant variation in how the velocity of the charged particle decreases. An additional effect is that at $\bar{t} = 0$, neutrals have no radial velocity component. But then, some neutrals develop a radial velocity upon colliding with charged particles, and in subsequent collisions, this neutral radial velocity can accelerate or decelerate the radial motion of charged particles. Figure 2(c) presents a simulation with a small $|\xi_i|$. The oscillations from cyclotron motion are visible in the radial motion because the collision frequency is much smaller than the cyclotron frequency. Even in this regime, the ion continues to move radially inwards, and Equation (12) still holds. In this low collisionality limit, the average radial velocity can be evaluated by averaging the jumps in guiding center $\Delta \mathbf{r}_{gc} = -\frac{1}{\omega_{c\sigma}} \hat{z} \times \Delta \mathbf{v}$ as a result of collisions; this corresponds to Equation (12) in the small $|\xi_\sigma|$ limit and yields an average guiding center radial velocity $v_{\sigma r} = \xi_\sigma u_{n\theta}$.

The radial velocity of neutrals is now derived from the conservation of total system CAM. Consider a collisional system where, at a specific radius, neutrals have density n_n and average azimuthal velocity $u_{n\theta}$, ions have density n_i and average azimuthal velocity $u_{i\theta}$, and electrons have density n_e and average azimuthal velocity $u_{e\theta}$. The CAM density at this

radius is thus

$$\begin{aligned} \mathcal{P}_\theta &= n_n m_n r_n u_{n\theta} + n_i m_i r_i u_{i\theta} + n_e m_e r_e u_{e\theta} \\ &+ \frac{1}{2} n_i q_i B r_i^2 + \frac{1}{2} n_e q_e B r_e^2 = \text{const.} \end{aligned} \quad (14)$$

During a small time Δt , the change of the CAM density is

$$\begin{aligned} \Delta \mathcal{P}_\theta &= n_n m_n (\Delta r_n u_{n\theta} + r_n \Delta u_{n\theta}) + n_i m_i (\Delta r_i u_{i\theta} + r_i \Delta u_{i\theta}) \\ &+ n_e m_e (\Delta r_e u_{e\theta} + r_e \Delta u_{e\theta}) + n_i q_i B r_i \Delta r_i \\ &+ n_e q_e B r_e \Delta r_e = 0. \end{aligned} \quad (15)$$

The system temporal evolution can be decomposed into two types of interspersed intervals, namely, time intervals where there are collisions and time intervals where there are no collisions. Only the time intervals when there are collisions could contribute to angular momentum transport between charged particles and neutrals. Because the two particles involved in a collision have the same r at the time of their collision and because there is no change in the total momentum of these two particles as a result of the collision, $n_n m_n r_n \Delta u_{n\theta} + n_i m_i r_i \Delta u_{i\theta} + n_e m_e r_e \Delta u_{e\theta} = 0$. Ignoring $n_i m_i \Delta r_i u_{i\theta} + n_e m_e \Delta r_e u_{e\theta}$ because it is much smaller than the magnetic parts of the CAM, Equation (15) reduces to

$$n_n m_n \Delta r_n u_{n\theta} + n_i q_i B r_i \Delta r_i + n_e q_e B r_e \Delta r_e = 0. \quad (16)$$

Assuming $u_{n\theta} = v_K = \sqrt{GM/r_n}$ and dividing by Δt , the radial velocity of neutrals is obtained as

$$u_{nr} = -\frac{\omega_{ci} m_i}{\omega_K m_n} (\chi_i u_{ir} - \chi_e u_{er}) \quad (17)$$

where $\chi_i = \frac{n_i}{n_n}$ and $\chi_e = \frac{n_e}{n_n}$ are the ion and electron density fractions. Assuming $\chi_i = \chi_e = \chi$, then

$$u_{nr} = -\chi \frac{\omega_{ci} m_i}{\omega_K m_n} (u_{ir} - u_{er}). \quad (18)$$

Using Equation (12), this becomes

$$u_{nr} = -\chi \omega_{ci} \frac{m_i}{m_n} \left(\frac{\xi_i}{1 + \xi_i^2} - \frac{\xi_e}{1 + \xi_e^2} \right) r_n. \quad (19)$$

Although we assume a uniform magnetic field for the sake of simplicity, the radial velocity expression still holds for a nonuniform magnetic field situation.

Figure 3(a)–(b) presents the radial motion of 43,022 neutrals, 440 ions, and 440 electrons initially uniformly distributed between $\bar{r} = 0.95$ and $\bar{r} = 2$ while Figure 3(c)–(d) shows, for comparison, a reference situation having neutrals only (no charged particles). These simulations have an initial velocity that is Kepler plus a small random velocity (essential for collisions to occur in the neutral-only reference case since without random velocities, neutrals in circular Keplerian orbits would never collide with each other). Figure 3(e)–(f) compares the u_{nr} dependence on r from the simulation with the prediction calculated from u_{ir} and u_{er} using Equation (17). The electric field generated from the charge separation is presumed to be small and is ignored in the simulation. The slight jaggedness of the prediction (circles) is because of the limited number of charged particles in each radius bin. The u_{nr} from the simulation has excellent agreement with the Equation (17) prediction in Figure 3(f) between $\bar{r} = 1$ and $\bar{r} = 1.8$ where the density fraction of charged particles is relatively stable. In

contrast, Figure 3(h) shows that when there are no charged particles, u_{nr} is zero in the central region, and there is only a small diffusive flux at the edges associated with the density gradient. Comparison between Figures 3(f) and (h) of u_{nr} in the interior region $1 < \bar{r} < 1.8$, (i.e., no edge diffusion) clearly shows that there is a substantial radial inward neutral flow only when charged particles are present. For the system with ions and electrons, the total system CAM is conserved with $\bar{P}_\theta = 5.4 \times 10^4$ while the total system OAM decreases from $\bar{L}_\theta(\bar{r} = 0) = 5.4 \times 10^4$ to $\bar{L}_\theta(\bar{r} = 0.8) = 3.7 \times 10^4$. For the neutrals-only system, the total system OAM is conserved with $\bar{L}_\theta(\bar{r} = 0) = \bar{L}_\theta(\bar{r} = 0.8) = 5.4 \times 10^4$.

The simulation conserves the total energy $W = \text{sum of kinetic and potential energies}$. For a single particle in a pure circular Keplerian orbit, the total energy in dimensioned parameters is $W = L^2/(2mr^2) - mM_*G/r = -mM_*G/(2r)$; thus, total energy would not be conserved if a particle moved from a pure circular Keplerian orbit at one radius to a pure circular Keplerian orbit at a different radius. Consequently, particles cannot change radius while simultaneously conserving energy and maintaining a pure circular Keplerian orbit. In a real disk, the energy released from the decrease of particle radial position would be extracted as blackbody radiation and electrical power expended in driving the astrophysical jets. This energy release from the disk would enable particles to maintain nearly circular Keplerian orbits as their radial position decreased. If it is assumed that particles maintain a pure circular Keplerian orbit as their radius decreases, Equation (17) becomes modified to give a u_{nr} that is double that of Equation (17); this comes from assuming that $n_n m_n \Delta(r_n u_{n\theta}) = \frac{1}{2} n_n m_n u_{n\theta} \Delta r_n$, since for a pure circular Keplerian orbit, $u_{n\theta} \sim r^{-1/2}$ and $n_n m_n r_n \Delta u_{n\theta} = -\frac{1}{2} n_n m_n u_{n\theta} \Delta r_n$.

The mass accretion rate is $\dot{M} = -2\pi r v_{nr} \Sigma$ where $\Sigma \approx n m_n h$ is the surface density and h is the scale height. Using the radial velocity of neutrals given by Equation (19), the accretion rate is thus

$$\dot{M} = 2\pi \chi n r^2 h |qB| \left(\frac{|\xi_i|}{1 + \xi_i^2} + \frac{|\xi_e|}{1 + \xi_e^2} \right). \quad (20)$$

The friction collision frequency between charged particles and neutrals taking into account dipole moment effects of neutrals is $\nu_{on} = \frac{m_n}{m_n + m_\sigma} n_n \langle \sigma v \rangle_{on}$ where typical values of the rate coefficients are $\langle \sigma v \rangle_{in} = 1.9 \times 10^{-9} \text{ cm}^3 \text{ s}^{-1}$ and $\langle \sigma v \rangle_{en} = 1.0 \times 10^{-15} \text{ cm}^2 \left(\frac{128kT_e}{9\pi m_e} \right)^{\frac{1}{2}}$ (Draine et al. 1983). At $r = 1 \text{ au}$, we presume $n_n = 10^{20} \text{ m}^{-3}$ (Hayashi 1981), $B = 5 \text{ mG}$ (Harrison et al. 2021), $\chi = 10^{-12}$ (Ilgner & Nelson 2006; Walsh et al. 2012), $T_e = 100 \text{ K}$, $h = 0.1 \text{ au}$, $m_i = m_H = 1.66 \times 10^{-27} \text{ kg}$, and $m_n = m_{H_2} = 3.32 \times 10^{-27} \text{ kg}$. Then $|\xi_i| = 2627$ and $|\xi_e| = 9.44$. Since $|\xi_i| \gg |\xi_e| \gg 1$ Equation (20) gives the mass accretion rate as $\dot{M} = 2\pi \chi n r^2 h |qB| / \xi_e = 2.9 \times 10^{-8} M_\odot \text{ yr}^{-1}$. This agrees well with observations that the mass accretion rate is $10^{-9} - 10^{-7} M_\odot \text{ yr}^{-1}$.

The accumulation of ions at small radius and accumulation of electrons at large radius establishes a radial electric field $E_r > 0$. The radial inward motion of the ions and outward motion of the electrons corresponds to a radial electric current $J_r < 0$. Because $E_r J_r < 0$, the process acts as an electric generator and so is a dynamo that converts gravitational potential energy into electrical energy. The radial electric field

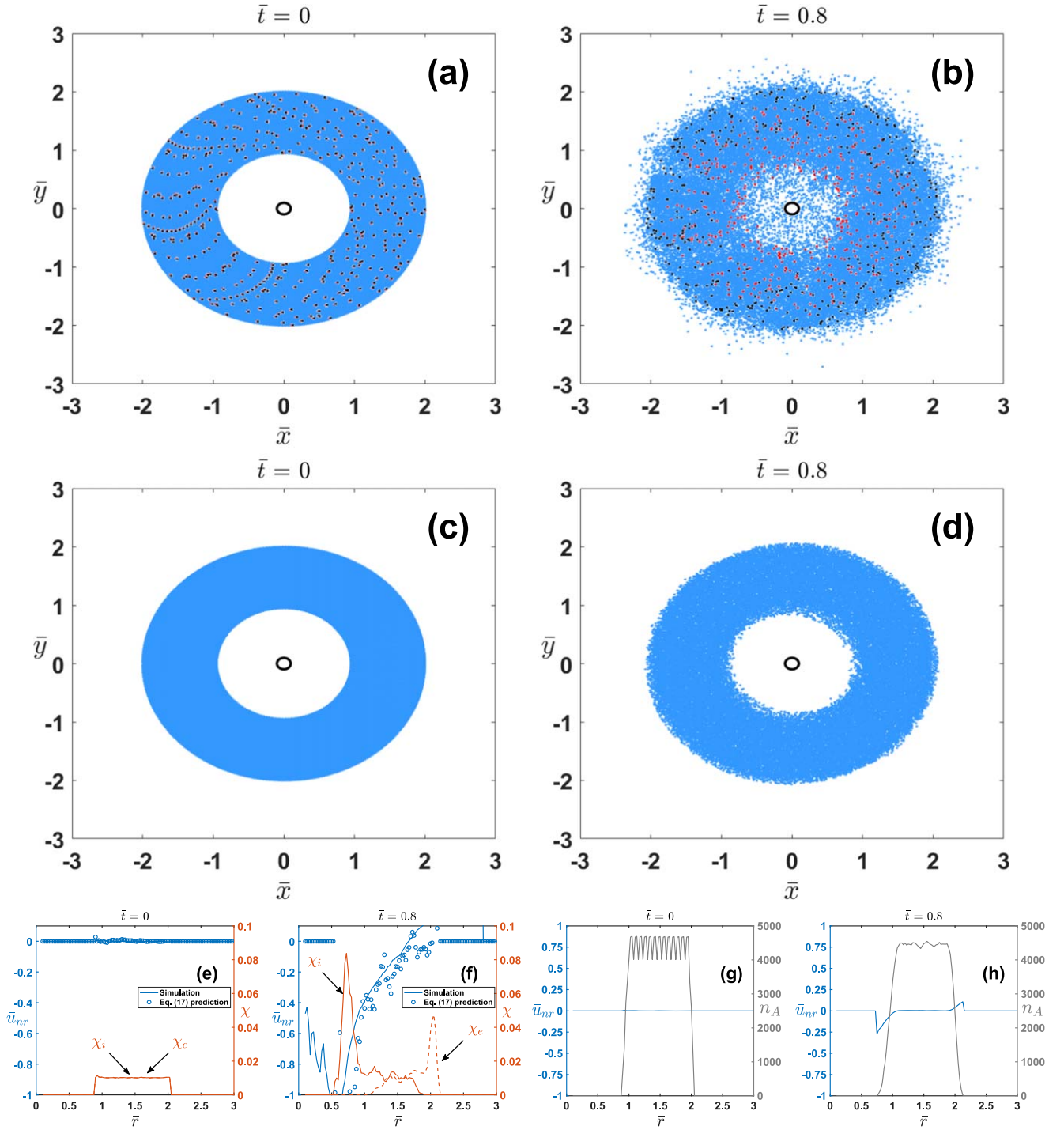


Figure 3. (a), (b) The particle trajectories of a system with ions and electrons at times $\bar{t} = 0$ and 0.8. The simulation has $\bar{a} = 3 \times 10^{-3}$, $\bar{d} = 5\bar{a}$, and $\bar{\omega}_{ci} = -50$ with $N_n = 43,022$ neutrals, $N_i = 440$ ions, and $N_e = 440$ electrons located in concentric circles ranging from $\bar{r} = 0.95$ to $\bar{r} = 2$. The ions and electrons are initially in adjacent pairs separated by a small azimuthal angle. The initial velocity is a Kepler velocity plus a random thermal velocity having 10% of the Kepler velocity magnitude, that is $\bar{\mathbf{v}}(\bar{t} = 0) = \sqrt{1/\bar{r}}\hat{\theta} + 0.1\sqrt{1/\bar{r}}\hat{\mathbf{v}}_{\text{random}}$ where $\hat{\mathbf{v}}_{\text{random}}$ is a random direction vector. The trajectories of the neutrals, ions, and electrons from $\bar{t} = 0$ to 0.8 are provided in the first part of the animation. (c), (d) The particle trajectories of a reference system having neutrals only at times $\bar{t} = 0$ and 0.8 with the same initial condition for neutrals as in (a). The trajectories from $\bar{t} = 0$ to 0.8 of the system with neutrals only appear immediately after the animation of the system with neutrals, ions, and electrons. (e), (f) The neutral radial drift velocity profile and the density fraction of ions and electrons of the system in (a), (b). The blue line is the radial drift velocity profile of neutrals obtained from the simulation. The average radial velocity at a certain radius \bar{r} is obtained as the average velocity of particles that are in a bin between radial position $\bar{r} - \Delta\bar{r}$ and $\bar{r} + \Delta\bar{r}$ with $\Delta\bar{r} = 0.05$. The blue circles are the radial velocity of neutrals calculated as a function of the ion radial velocity and electron radial velocity as predicted by Equation (17). The red solid/dashed line shows the ion/electron density fraction vs. radial position. (g), (h) The neutral drift velocity profile and neutral surface density n_A vs. radial position of the system of (c), (d). The rippling of n_A in (g) is from the aliasing of the radial position bin period and the concentric circle position period; this rippling smooths out as the random velocity and collisions destroy the imposed initial pattern of concentric circles of neutrals.

(An animation of this figure is available.)

provides an electric force that opposes the radial inward motion of the ions and outward motion of the electrons. The maximum radial electric field on the disk plane $E_{r\max} = -Bu_{n\theta} = -B\sqrt{\frac{GM_*}{r}}$ is achieved when the charge accumulation stops; this maximum will occur if there is no means to drain the charge accumulation, and at this maximum radial electric field, the time-average radial velocity of charged particles goes to zero so the electric current would cease. However, if a mechanism such as an astrophysical jet circuit exists to drain the charge accumulation, the radial electric field in the $z=0$ plane will drive an out-of-plane electric current; this electric field will be less than $E_{r\max}$. The bidirectional jet electric currents are directed away from the accretion disk in the small radius region (ion accumulation region). The slight r component of the out-of-plane electric current and its associated azimuthal magnetic field B_ϕ produce $J_r B_\phi$ forces that drive bidirectional astrophysical jets flowing away from the disk plane; this adds to axial pressure gradients that also drive a flow away from the disk plane (Bellan 2016, 2020). This jet generation configuration is topologically analogous to the Caltech astrophysical jet experiment (Hsu & Bellan 2002; You et al. 2005; Kumar & Bellan 2009) where a poloidal current is produced by a power supply imposing a radial electric field between a conducting disk in the $z=0$ plane and a coplanar conducting annulus surrounding the disk and separated by a small gap.

4. Conclusions

(i) The fundamental conserved quantity is the canonical angular momentum $mr v_\theta + q\psi/2\pi$, not the ordinary angular momentum $mr v_\theta$. Ordinary angular momentum and canonical angular momentum are identical for a neutral but are very different for charged particles.

(ii) Collisions transfer neutral ordinary angular momentum to charged particle canonical angular momentum, so neutrals spiral inward.

(iii) The accumulation of ions at small radius and electrons at large radius creates a radial electric field. Since $E_r J_r < 0$, the disk acts as a gravity-powered dynamo.

(iv) The accumulation of ions at small radius drives an axially outward out-of-plane poloidal electric current along the poloidal magnetic field at small radius. This current and its associated magnetic field produce forces that drive bidirectional astrophysical jets flowing away from the disk. The increasing energy in the jets as they lengthen is powered by the gravitational disk dynamo.

This material is based upon work supported by NSF award Nos. 2105492 and 1914599.

ORCID iDs

Yang Zhang  <https://orcid.org/0000-0002-4168-9225>
Paul M. Bellan  <https://orcid.org/0000-0002-0886-8782>

References

- Balbus, S. A. 2003, *ARA&A*, 41, 555
Balbus, S. A., & Hawley, J. F. 1991, *ApJ*, 376, 214
Bellan, P. M. 2016, *MNRAS*, 458, 4400
Bellan, P. M. 2020, *ApJ*, 888, 69
Boris, J. 1970, in Proc. Fourth Conf. on Numerical Simulation of Plasmas, ed. J. P. Boris & R. A. Shanny (Washington, DC: Naval Research Laboratory), 3
Draine, B. T., Roberge, W. G., & Dalgarno, A. 1983, *ApJ*, 264, 485
Flaherty, K. M., Hughes, A. M., Rose, S. C., et al. 2017, *ApJ*, 843, 150
Gullbring, E., Hartmann, L., Briceno, C., & Calvet, N. 1998, *ApJ*, 492, 323
Harrison, R. E., Looney, L. W., Stephens, I. W., et al. 2021, *ApJ*, 908, 141
Hayashi, C. 1981, *PTPhS*, 70, 35
Hsu, S. C., & Bellan, P. M. 2002, *MNRAS*, 334, 257
Ilgner, M., & Nelson, R. P. 2006, *A&A*, 445, 205
Ji, H., & Balbus, S. 2013, *PhT*, 66, 27
Ji, H., Burin, M., Schartman, E., & Goodman, J. 2006, *Natur*, 444, 343
Kumar, D., & Bellan, P. M. 2009, *PhRvL*, 103, 105003
Shakura, N. I., & Sunyaev, R. A. 1973, *A&A*, 24, 337
You, S., Yun, G., & Bellan, P. M. 2005, *PhRvL*, 95, 045002
Walsh, C., Nomura, H., Millar, T., & Aikawa, Y. 2012, *ApJ*, 747, 114